Designing custom medium resolution observing modes to trace planet accretion with SCALES

Raquel A. Martinez[a], Steph Sallum[a], Ravinder Banyal[b], Natalie Batalha[c], Natasha Batalha[d], Geoff Blake[e], Tim Brandt[f], Zack Briesemeister[g], Katherine de Kleer[e], Imke de Pater[h], Aditi Desai[a], Josh Eisner[i], Wen-fai Fong[j], Tom Greene[d], Mitsuhiko Honda[k], Isabel Kain[c], Charlie Kilpatrick[j], Renate Kupke[l], Mackenzie Lach[a], Mike Liu[m], Bruce Macintosh[l], Dimitri Mawet[e,n], Brittany Miles[i], Caroline Morley[o], Diana Powell[p], Patrick Sheehan[q], Andrew J. Skemer[c], Justin Spilker[r], Deno Stelter[l], Jordan Stone[s], Arun Surya[t], Sivarani Thirupathi[b], Kevin Wagner[i], and Yifan Zhou[u]

[a]University of California, Irvine, Irvine, CA USA
[b]Indian Institute of Astrophysics, Bangalore, India
[c]University of California, Santa Cruz, Santa Cruz, CA, USA
[d]NASA Ames Research Center, Moffett Field, CA, USA
[e]California Institute of Technology, Pasadena, CA, USA
[f]University of California, Santa Barbara, Santa Barbara, CA, USA
[g]NASA Goddard Space Flight Center, Greenbelt, MD, USA
[h]University of California, Berkeley, Berkeley, CA, USA
[i]University of Arizona, Tucson, AZ, USA
[j]Northwestern University, Evanston, IL, USA
[k]Okayama University of Science, Okayama, Japan
[l]University of California Observatories, Santa Cruz, CA, USA
[m]University of Hawai'i, Honolulu, HI, USA
[n]Jet Propulsion Laboratory, Pasadena, CA, USA
[o]The University of Texas at Austin, Austin, TX, USA
[p]University of Chicago, Chicago, IL, USA
[q]National Radio Astronomy Observatory, Charlottesville, VA, USA
[r]Texas A&M University, College Station, TX, USA
[s]Naval Research Laboratory, Washington, DC, USA
[t]Tata Institute of Fundamental Research, Mumbai, India
[u]The University of Virginia, Charlottesville, VA, USA

ABSTRACT

The Slicer Combined with Array of Lenslets for Exoplanet Spectroscopy (SCALES) is an under-construction thermal infrared high-contrast integral field spectrograph that will be located at the W. M. Keck Observatory. SCALES will detect and characterize planets that are currently inaccessible to detailed study by operating at thermal (2–5 μm) wavelengths and leveraging integral-field spectroscopy to readily distinguish exoplanet radiation from residual starlight. SCALES' wavelength coverage and medium-spectral-resolution ($R \sim 4{,}000$) modes will also enable investigations of planet accretion processes. We explore the scientific requirements of additional custom gratings and filters for incorporation into SCALES that will optimally probe tracers of accretion in forming planets. We use ray-traced hydrogen emission line profiles (i.e., Brγ, Brα) and the SCALES end-to-end simulator, `scalessim`, to generate grids of high-fidelity mock datasets of accreting planetary systems

Further author information: (Send correspondence to Raquel A. Martinez)
E-mail: r.martinez@uci.edu

Techniques and Instrumentation for Detection of Exoplanets XI, edited by Garreth J. Ruane, Proc. of SPIE Vol. 12680, 126801W · © 2023 SPIE
0277-786X · doi: 10.1117/12.2677530

with varying characteristics (e.g., $T_{\rm eff}$, planet mass, planet radius, mass accretion rate). In this proceeding, we describe potential specialized modes that best differentiate accretion properties and geometries from the simulated observations.

Keywords: instrumentation: thermal infrared, integral field spectroscopy, simulation

1. INTRODUCTION

Our current understanding of exoplanet atmospheres mostly comes from ground-based near-infrared (1–2 μm) photometry and spectroscopy. However, most self-luminous exoplanets emit the majority of their radiation in the thermal-infrared[1] (2–5 μm). The Slicer Combined with Array of Lenslets for Exoplanet Spectroscopy (SCALES; see Skemer et al. 2022[2]) will leverage this fact to observe exoplanets where they are brightest, while also utilizing integral-field spectroscopy to distinguish between exoplanet light and residual starlight via spectral-differential imaging.[3] Other key science drivers for SCALES include: protoplanetary disk characterization, Solar System object monitoring, supernova remnant mapping, and active galactic nuclei characterization. See Sallum et al. (2023)[4] in these proceedings for further information regarding SCALES' science goals.

SCALES will use a custom silicon lenslet array, changeable coronagraphs, and dispersive prisms to carry out integral-field spectroscopy over a $2.2'' \times 2.2''$ field of view for its low spectral resolution ($R < 300$) modes. A small 17×18 lenslet array portion with a $0.34'' \times 0.36''$ field-of-view will be placed onto an advanced image slicer for medium resolution observing at $R \approx 3{,}500 - 7{,}000$ (see Figure 1). This subarray will be reconfigured into a pseudo-slit then dispersed across the full SCALES H2RG detector. A piezo mirror will steer the intended science target onto the lenslet subarray and hold it there for the duration of an observation. SCALES' baseline medium resolution modes will cover each of the K, L, and M bands with spectral resolution determined by available detector space (see Table 1). Stelter et al. (2022),[5] also Stelter et al. (2023) in these proceedings,[6] has a full discussion of the SCALES medium-resolution design. These modes at thermal infrared wavelengths meet high-level science requirements to constrain molecular abundances of methane, ammonia, carbon monoxide, and water vapor in exoplanet atmospheres.

SCALES will characterize exoplanets at longer wavelengths than current high-contrast integral-field spectrographs (IFS; e.g., GPI,[7] SPHERE,[8] CHARIS,[9] ALES[10]). This will enable the study of planet populations that have thus far not been accessible to detailed study, specifically colder (<700 K) exoplanets. The youngest exoplanets for a given mass are easiest to detect because they are radiating away residual heat from their recent formation,[11,12] which is why near-infrared direct-imaging searches typically target star-forming regions and young moving groups. These studies have thus far resulted in low yields,[13–15] suggesting that gas-giant planets are rare. However, constraints on giant planet occurrence frequency are heavily dependent upon the models assumed for planet population distributions, initial entropy, and thermal evolution. For instance, exoplanets formed via core accretion with a "cold-start"[16] are theorized to have initial luminosities much lower than planets produced through cloud fragmentation, disk instabilities, or core accretion with planetary surface shocks ("hot-start" models[17–20]). This suggests there may be a hypothetical population of "cold-start" planets that are undetectable with near-infrared IFSs but to which SCALES would be sensitive.

SCALES will also be able to observe actively-forming exoplanets embedded in their nascent disks by distinguishing between circumstellar disk scattered light and protoplanet emission. In fact, detecting these systems offers the opportunity to witness planet assembly and circumplanetary disk evolution in action, as evidenced by the detection of accretion tracers for known protoplanets.[21–23] Accretion onto forming planets produces observable signatures in their spectra in the form of ultraviolet radiation excess and hydrogen emission line features. While shocked infalling gas produces excess UV flux that traces accretion directly, observing in the UV from ground-based telescopes is difficult; instead, optical H lines (i.e., Hα) are typically used as proxies.[24] However, these are prone to large systematic uncertainties from non-accretion processes, such as chromospheric activity[25] and extinction from circumstellar or circumplanetary material.[26] Infrared emission lines (i.e., the Paschen and Brackett series) suffer less dust extinction and also do not suffer as much chromospheric emission contamination as lower-excitation lines do.[27,28] Therefore, SCALES may enable more robust accretion diagnostics in forming exoplanets, provided that planetary accretion luminosities in these lines are high enough to be detectable.[29–32]

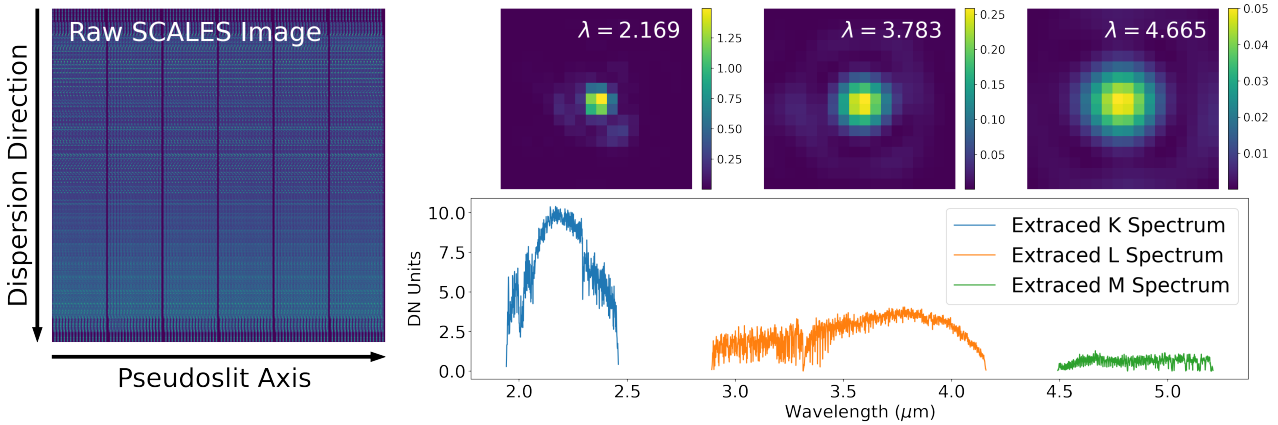

Figure 1. Medium-resolution observation of a 2000 K brown dwarf in the K-, L-, and M-bands created using `scalessim`. Left panel: Raw K-band image of the SCALES H2RG detector with spectra dispersed onto it. Top right three panels: Extracted PSFs from a slice of `scalessim`-generated data cubes in each of the medium-resolution filters. Right panel: Extracted spectra from a 1 s exposure using an aperture with radius of 4 pixels.

In the future, we anticipate the ability to upgrade SCALES with additional higher resolution gratings. This paper describes our exploration of such gratings that would detect and characterize the accretion signatures from protoplanets. We test modes that would enable SCALES to not only trace accretion in forming planets, but also constrain the properties of the accretion flow from observational signatures (i.e., emission line profiles). In order to simulate realistic observations of these science targets, we add functionality to `scalessim`, the SCALES end-to-end simulator,[33] that includes changing sky conditions for observation planning purposes as well as adjustable grating dispersion curves.

Table 1. SCALES Medium Resolution Mode Specifications

Wavelength Range	Band	Resolving Power
1.95–2.45 μm	K	~5,000
2.9–4.15 μm	L	~3,500
4.5–5.2 μm	M	~7,000

2. GRATING REQUIREMENTS

The SCALES end-to-end simulator, `scalessim`,[33] was created to investigate of the impacts of optomechanical design choices on SCALES science outcomes. The `scalessim` software includes actual dispersion curves for SCALES' low-resolution prisms, but currently assumes linear dispersion for the medium-resolution gratings. These linear dispersion files are used to calculate the position at which monochromatic lenslet point spread functions (PSFs) are imaged onto the SCALES detector. The `scalessim` software includes medium-resolution dispersion files that are tuned to the K, L, and M bands with spectral resolutions of ~5,000, ~3,500, and ~7,000, respectively. The mock IFS data cube output from `scalessim` is generated as if perfect spectral extraction has been performed on the raw SCALES detector images (i.e., perfect deconvolution of the SCALES PSF occurs so that all flux from the detector is collected). The data cube can be oversampled in wavelength but then summed and binned to the appropriate spectral resolution.

In order to explore SCALES' ability to constrain accretion physics, we generated new dispersion files with $R = 10{,}000$ in the K and L bands centered on the Brγ (2.165 μm) and Brα (4.051 μm) hydrogen emission line wavelengths—two important accretion tracers that SCALES will be able to detect in forming exoplanets.[31,34]

The higher resolution dispersion modes require slightly different bandpasses due to detector space. SCALES' medium-resolution mode will operate from 1.95–2.45 μm in the K-band and from 2.9–4.15 μm in the L-band. The higher resolution modes explored here would operate from 2.06–2.27 μm in the K-band and from 3.86–4.24 μm in the L-band. We chose to center the higher resolution L-band mode on the Br α emission line just for simulation purposes, but we note that the Earth's atmosphere is opaque from 4.15–4.45 μm and our final custom mode in the L-band will be shifted (see Sec. 5). We provide `scalessim` with Keck PSF cubes that range in wavelength from 1.9–5.3 μm with $\Delta\lambda = 0.0001$ μm ($R \sim 40{,}000$ at 4 μm) and bin the resultant simulated observations down to R of 10,000. We also experiment with binning the observations down to R of 20,000 and keeping R at 40,000 to further explore even higher resolution modes and any trade offs in line profile fitting (see Section 4).

3. SIMULATED OBSERVATIONS

We use `scalessim` to generate high-fidelity mock medium-resolution datasets. The simulation architecture processes astrophysical fields into IFS data cubes that can be analyzed and interpreted by the user. Users provide atmospheric conditions and observation patterns (i.e., exposure time, slew to background, slew to flux calibrator or telluric standard) to create individual exposures. The `scalessim` software is written in Python and tutorial notebooks are available on `github`.*

3.1 Protoplanet Observations

We use the TORUS radiative transfer code[35] to model the Brα and Brγ hydrogen line profiles of a 1 $M_{\rm Jup}$ protoplanet with 1.56 $R_{\rm Jup}$ radius at 150 pc undergoing magnetospheric accretion with inner radius equal to 1.5 $R_{\rm p}$. We generate a grid of line profiles varying accretion rate ($\dot{M}$), inclination angle (i), and the outer radius of the protoplanet's magnetosphere (R_{outer}; see Table 2). These line profiles are then run through `scalessim` to generate data cubes for 120-s exposures. For this work, we choose to work with 120-s exposures to avoid sky saturation. A total of 142 exposures are generated for a total integration time of 284 min. This represents observing one science target for a full night of observing, including nodding off-target for 120-s sky background observations after each science exposure and taking a 120-s exposure of an A0 flux calibrator every hour. We use `scalessim` to include sky background and transmission in the generation of mock data with the same 120-s exposure and add Poisson noise prior to spectral extraction. Spectra are extracted from the 3-D data cubes with aperture photometry using a 4-pixel radius centered on the target (see Figure 2). Dedicated sky background and telluric calibrator data cubes were generated in the above fashion to perform sky subtraction and flux calibration.

3.2 Sky Conditions and Observing Cadence

Previously, `scalessim` required explicit definitions of precipitable water vapor (PWV) and airmass (z) that were then rounded to discrete values (1.0, 1.6, 3.0, 5.0 mm for PWV; 1.0, 1.5, 2.0 for z) for which theoretical sky background and transmission spectral models are available, calculated with the atmospheric model ATRAN[36] by the Gemini Observatory.† We developed a new module for `scalessim` that allows users to generate observations with any value of PWV below 5 mm and z between 1 and 2 when generating sky background and transmission

Table 2. TORUS Line Profile Grid Summary

Parameter	Symbol	Units	Range	Δ
Accretion Rate	$\dot{M}$	$M_{\rm Jup}$ yr^{-1}	$[10^{-6}, 10^{-3}]$	10^{-1}
Outer Disk	R_{outer}	$R_{\rm p}$	[3, 6]	3
Inclination	i	$^\circ$	[0, 90]	30

*`scalessim` can be found at: https://github.com/scalessim/scalessim. Increasing the resolution of the SCALES grating required small adjustments to some `scalessim` modules and functions which will also be made publicly available.

†https://www.gemini.edu/observing/telescopes-and-sites/sites

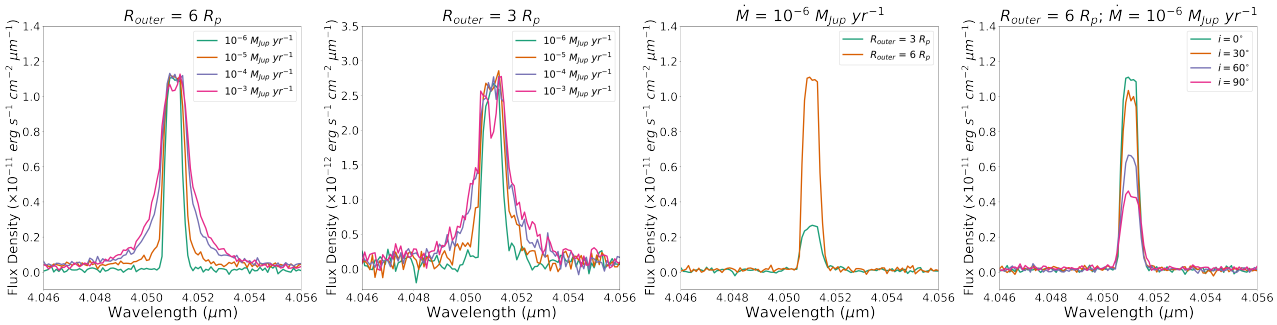

Figure 2. Simulations of a 284-min integration of Brα line profiles for a 1 $M_{\rm Jup}$ protoplanet with $R_{\rm p}$=1.56 $R_{\rm Jup}$ and inner magnetosphere radius of 1.5 $R_{\rm p}$ in the L band. TORUS-produced line profiles are used as input for `scalessim` to produce mock data sets that include sky background and transmission. The spectra were extracted from the generated data cubes using an aperture with radius of 4 pixels and flux calibrated using an A0 star.

realizations. The new module reads in the sky background (or transmission) spectral models at the sparsely-sampled values of PWV and z to create a two-dimensional parameter surface, then uses bilinear interpolation to generate a new sky model at the user-specified PWV and z values.

Looking forward to science commissioning and SCALES observing community needs, we have also generated Python-based observation planning notebooks. The notebooks allow users to determine the actual z values of a science or calibration target for the duration of an observing night utilizing `astroplan`.[37] Users can also sample historical PWV measurements for an "excellent", "very good", and "fair" night of observing at Maunakea (see Fig. 3) calculated from τ_{225} measurements archived by the Caltech Submillimeter Observatory.[‡] We use this functionality to explore the impacts of increasing the cadence of observing telluric standards during the night on flux calibration. We create data cubes of an A0 standard star exposed for 120 s at the beginning and end of the observing night (∼4.5 hr apart), as well as at intervals of 60 min and 15 min. The PWV curves shown in Figure 3 and `astroplan` predicted z values are then sampled to determine pairs of PWV and z to be put into `scalessim` at the respective cadence times. Incorporating realistically changing sky conditions and

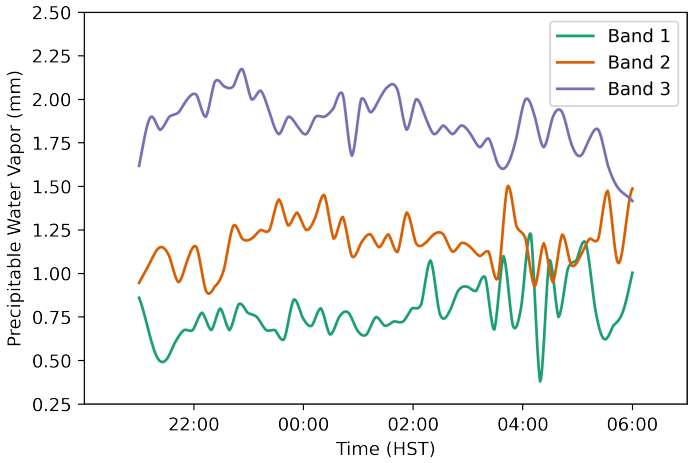

Figure 3. Band 1 (<0.83 mm), Band 2 (0.83–1.58 mm), and Band 3 (1.58–2.58 mm) PWV conditions for "excellent", "very good", and "fair" nights of observing at Maunakea. Values were calculated from τ_{225} measurements archived by the Caltech Submillimeter Observatory.

[‡] http://cso.caltech.edu/tau/

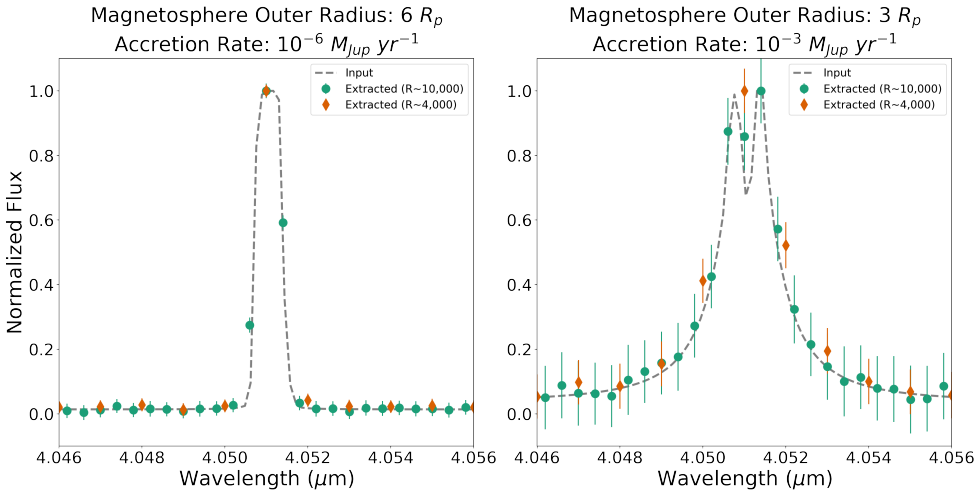

Figure 4. Comparison between the extracted spectra from the current SCALES medium-resolution observing mode (orange diamonds) and that of our custom $R = 10,000$ observing mode (green circles). The current SCALES medium resolution mode can detect hydrogen line emission from magnetospheric accretion but does not adequately sample the input profile, especially for protoplanets with higher accretion rates and/or smaller accretion disks. Left-hand panel: Expected Brα emission from a 1 $M_{\rm Jup}$ protoplanet with $R_{\rm p}$=1.56 $R_{\rm Jup}$, inner magnetosphere radius of 1.5 $R_{\rm p}$, outer magnetosphere radius of 6 $R_{\rm p}$, $\dot{M} = 10^{-6}$ $M_{\rm Jup}$ yr^{-1}, and $i = 0°$ (gray dashed line). Right-hand panel: Expected Brα emission from a 1 $M_{\rm Jup}$ protoplanet with $R_{\rm p}$=1.56 $R_{\rm Jup}$, inner magnetosphere radius of 1.5 $R_{\rm p}$, outer magnetosphere radius of 3 $R_{\rm p}$, $\dot{M} = 10^{-3}$ $M_{\rm Jup}$ yr^{-1}, and $i = 0°$ (gray dashed line).

target elevations into `scalessim` will enable observers to determine the best observing cadences and patterns to maximize their signal-to-noise goals with SCALES.

4. RESULTS

Figure 4 shows two example input Brα line profiles and extracted spectra for observations taken with SCALES' planned medium resolution mode and the custom $R \sim 10,000$ grating. We present Brα exclusively in this work but the trends seen are similar for simulated observations of Brγ. The first model shown (left-hand panel) is the expected Brα emission for an accreting protoplanet with an outer magnetosphere radius of 6 $R_{\rm p}$, $\dot{M} = 10^{-6}$ $M_{\rm Jup}$ yr^{-1}, and $i = 0°$. The second model shown (right-hand panel) has a different outer magnetosphere radius of 3 $R_{\rm p}$ and accretion rate of $\dot{M} = 10^{-3}$ $M_{\rm Jup}$ yr^{-1}. The total integration time for the simulated spectra is 284 min. The data have been flux calibrated using an A0 star and the line profiles have been normalized to the peak line intensity.

We also explore R of 10,000, 20,000, and 40,000 observing modes and their ability to constrain accretion parameters (for TORUS, $\dot{M}$, R_{outer}, i; see Figure 5). We focus our analysis on the TORUS models we generated with $\dot{M} = 10^{-5}$ $M_{\rm Jup}$ yr^{-1} and $\dot{M} = 10^{-6}$ $M_{\rm Jup}$ yr^{-1} since these are accretion rates that would form a giant planet in ∼10,000 to 1 Myr. We ran these TORUS line profiles through `scalessim` with individual exposure times of 120 s, PWV=0.8 mm, and $z = 1$. We created 51 individual frames for a total integration time on target of 102 min that simulates taking observations of a science target and nodding off to take sky background observations for half of an observing night. We performed aperture photometry on the simulated data cubes in the same manner as described in Section 3.1. We also extracted noiseless spectra of each TORUS model at each resolution to compare to our simulated observations and generate χ^2 statistics.

In Figure 5 we show how the simulated line profiles change at the different resolutions we explored. The extracted spectra are for a simulated observation of an accreting protoplanet with $R_{outer} = 6$ $R_{\rm p}$ and $\dot{M} = 10^{-6}$ $M_{\rm Jup}$ yr^{-1}. We also extract a noiseless spectrum of the TORUS line profile, as well as a noiseless spectrum of a TORUS line profile that has the outer magnetosphere radius changed to 3 $R_{\rm p}$. We then calculate the χ^2 between the simulated observation and the noiseless spectrum (i.e., the best-fit model), as well as the χ^2 between the

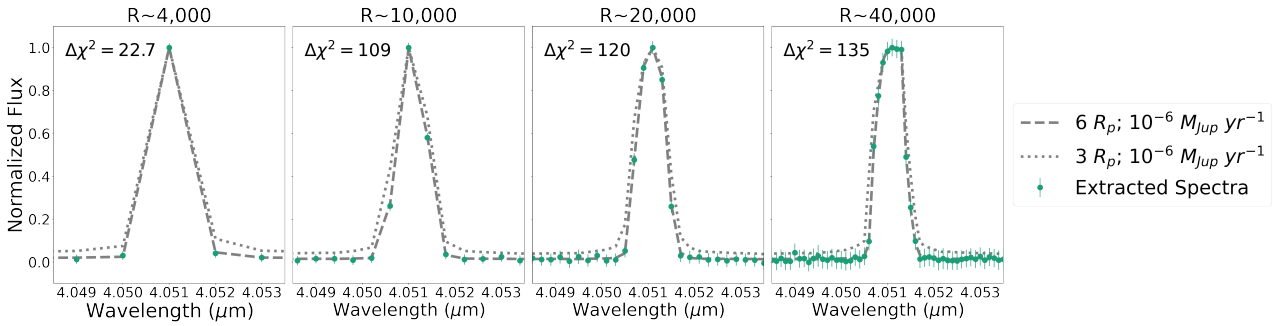

Figure 5. Simulated observations of a 1 $M_{\rm Jup}$ protoplanet with $R_{\rm p}$=1.56 $R_{\rm Jup}$, inner magnetosphere radius of 1.5 $R_{\rm p}$, outer magnetosphere radius of 6 $R_{\rm p}$, $\dot{M} = 10^{-6}$ $M_{\rm Jup}$ yr^{-1}, and $i = 0°$ (green circles) compared to modeled line profiles of an accreting object with $R_{outer} = 6$ $R_{\rm p}/\dot{M} = 10^{-6}$ $M_{\rm Jup}$ yr^{-1} (dashed line) and $R_{outer} = 3$ $R_{\rm p}/\dot{M} = 10^{-6}$ $M_{\rm Jup}$ yr^{-1} (dotted line) sampled at resolutions of 4,000, 10,000, 20,000 and 40,000. Each panel is labeled with the change in χ^2 between fitting the observations with the best-fit model ($R_{outer} = 6$ $R_{\rm p}$, $\dot{M} = 10^{-6}$ $M_{\rm Jup}$ yr^{-1}) and fitting the observations with one parameter changed ($R_{outer} = 3$ $R_{\rm p}$), indicating that increasing the resolution of the SCALES accretion-tracing mode also increases its constraining power.

simulated observation and the noiseless spectrum of a model with one parameter changed. As the resolution increases, we see that the $\Delta\chi^2$ between the best-fit model and a model with a magnetosphere radius of 3 $R_{\rm p}$ increases. This indicates that increasing the resolution of the SCALES accretion-tracing mode also increases its constraining power by excluding more models.

In Figure 6 we show the changes in χ^2 as one model parameter is varied with increased SCALES spectral resolution. We also indicate where $\Delta\chi^2 = 3.53$ in each panel, which is the value that signifies a 1-σ difference from the best-fit model for three degrees of freedom. The simulated observation shown is of a protoplanet with $R_{outer} = 3$ $R_{\rm p}$, $\dot{M} = 10^{-6}$ $M_{\rm Jup}$ yr^{-1}, and $i = 0°$, but the trends seen in the figures are similar for other simulated observations. In the leftmost panel, we changed the accretion rate from 10^{-6} $M_{\rm Jup}$ yr^{-1} to 10^{-5} $M_{\rm Jup}$ yr^{-1}. We see that we can easily constrain a 10× difference in $\dot{M}$ at R = 4,000, 10,000, 20,000 and 40,000. In

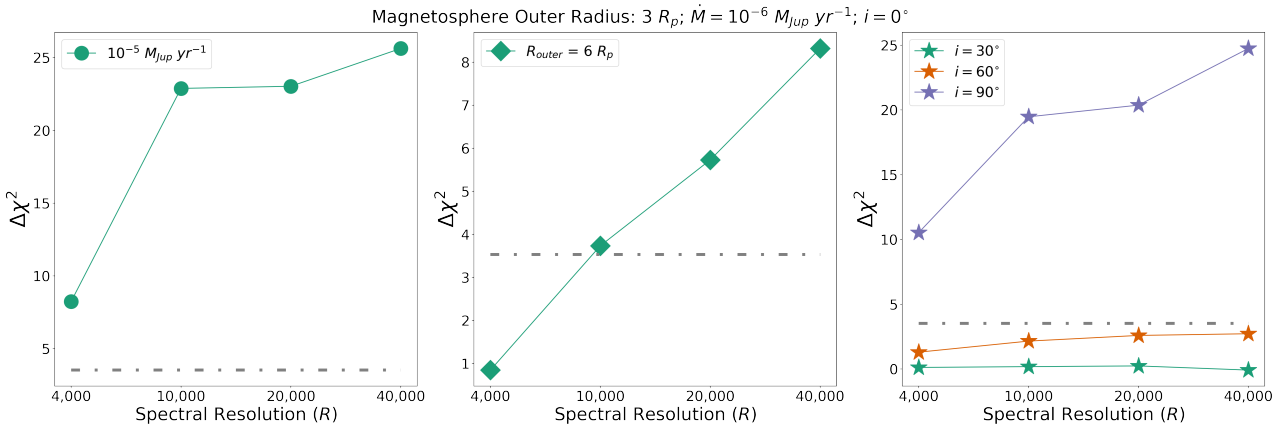

Figure 6. Change in χ^2 as one model parameter is varied with increased SCALES spectral resolution. Also indicated is where $\Delta\chi^2 = 3.53$ in each panel which is the value of $\Delta\chi^2$ that signifies a 1-σ difference from the best-fit model. The simulated observation shown is of a 1 $M_{\rm Jup}$ protoplanet with $R_{\rm p}$=1.56 $R_{\rm Jup}$, inner magnetosphere radius of 1.5 $R_{\rm p}$, outer magnetosphere radius of 3 $R_{\rm p}$, $\dot{M} = 10^{-6}$ $M_{\rm Jup}$ yr^{-1}, and $i = 0°$. Leftmost panel: A 10× difference in $\dot{M}$ at $R = 4,000$, 10,000, 20,000 and 40,000 is easily constrained. Middle panel: Only higher-resolution specialized modes ($R \geq 10,000$) can constrain the outer radius of the magnetosphere accretion disk. Rightmost panel: When fitting for inclination only $i \gtrsim 60°$ can be constrained in any of the medium-resolution modes explored.

the middle panel, we change R_{outer} from 3 R_p to 6 R_p. We see that only for higher-resolution specialized modes ($R \geq 10{,}000$) can the outer radius of the magnetosphere accretion disk be constrained. In the rightmost panel, we vary the inclination and see that we can only constrain differences in inclination greater than $\sim 60°$ across any of the medium-resolution modes explored.

5. FUTURE WORK

We note that the sky background at Maunakea will begin to dominate observations past 4.15 μm, causing saturation in exposure times not much longer than the 120 s observations used in this work. The final higher-resolution L-band grating will include the Brα wavelength, but not center it, to ensure high signal-to-noise observations of this emission line while avoiding saturating on sky. Consideration and incorporation of additional systematic noise sources (e.g., stellar halo for close companions, steering mirror pointing errors) into `scalessim` is needed to assess their impact on spectral extraction, which has implications for telluric and photometric calibration strategies. Also in future work, we will generate a larger, finer grid of TORUS line profiles to run through `scalessim` and more thoroughly assess parameter uncertainty impacts for custom observing modes. We will also perform this analysis with different models of accretion (i.e., Aoyama et al. 2018,[29] Marleau et al. 2022[32]) to see if additional considerations are required to finalize the design of a custom accretion-tracing mode. Additional validation of this work with previous on-sky Maunakea observations of accreting protoplanets and substellar objects will be pursued. These analyses will enhance SCALES' ability to differentiate between accretion paradigms when observing protoplanets.

ACKNOWLEDGMENTS

We gratefully acknowledge the Heising-Simons Foundation, the Alfred P. Sloan Foundation, and the Mt. Cuba Astronomical Foundation for their generous support of SCALES. RAM is supported by the National Science Foundation MPS-Ascend Postdoctoral Research Fellowship under Grant No. 2213312. SS is supported by the National Science Foundation under MRI Grant No. 2216481.

REFERENCES

[1] Skemer, A. J., Marley, M. S., Hinz, P. M., Morzinski, K. M., Skrutskie, M. F., Leisenring, J. M., Close, L. M., Saumon, D., Bailey, V. P., Briguglio, R., Defrere, D., Esposito, S., Follette, K. B., Hill, J. M., Males, J. R., Puglisi, A., Rodigas, T. J., and Xompero, M., "Directly Imaged L-T Transition Exoplanets in the Mid-infrared," **792**, 17 (Sept. 2014).

[2] Skemer, A. J., Stelter, R. D., Sallum, S., MacDonald, N., Kupke, R., Ratliff, C., Banyal, R., Hasan, A., Varshney, H. M., Surya, A., Prakaesh, A., Thirupathi, S., Sethuram, R., K. V., G., Fitzgerald, M. P., Wang, E., Kassis, M., Absil, O., Alvarez, C., Batalha, N., Boucher, M.-A., Bourgenot, C., Brandt, T., Briesemeister, Z., de Kleer, K., de Pater, I., Deich, W., Divakar, D., Filion, G., Gauvin, É., Gonzales, M., Greene, T., Hinz, P., Jensen-Clem, R., Johnson, C., Kain, I., Kruglikov, G., Lach, M., Landry, J.-T., Li, J., Liu, M. C., Lyke, J., Magnone, K., Marin, E., Martin, E., Martinez, R., Mawet, D., Miles, B., Sandford, D., Sheehan, P., Sohn, J. M., and Stone, J., "Design of SCALES: a 2-5 micron coronagraphic integral field spectrograph for Keck Observatory," in [*Ground-based and Airborne Instrumentation for Astronomy IX*], Evans, C. J., Bryant, J. J., and Motohara, K., eds., *Society of Photo-Optical Instrumentation Engineers (SPIE) Conference Series* **12184**, 121840I (Aug. 2022).

[3] Smith, W. H., "Spectral differential imaging detection of planets about nearby stars.," **99**, 1344–1353 (Dec. 1987).

[4] Sallum, S. *Society of Photo-Optical Instrumentation Engineers (SPIE) Conference Series* (2023).

[5] Stelter, R. D., Skemer, A. J., Kupke, R., Bourgenot, C., Martinez, R. A., and Sallum, S. S., "Weighing exo-atmospheres: a novel mid-resolution spectral mode for SCALES," in [*Ground-based and Airborne Instrumentation for Astronomy IX*], Evans, C. J., Bryant, J. J., and Motohara, K., eds., *Society of Photo-Optical Instrumentation Engineers (SPIE) Conference Series* **12184**, 1218445 (Aug. 2022).

[6] Stelter, R. D. *Society of Photo-Optical Instrumentation Engineers (SPIE) Conference Series* (2023).

[7] Macintosh, B. A., Anthony, A., Atwood, J., Bauman, B., Cardwell, A., Caputa, K., Chilcote, J., De Rosa, R. J., Dillon, D., Doyon, R., Dunn, J., Erickson, D., Fitzgerald, M. P., Gavel, D. T., Galvez, R., Goodsell, S., Graham, J., Greenbaum, A. Z., Hartung, M., Hibon, P., Ingraham, P., Kerley, D., Konopacky, Q., Labrie, K., Larkin, J., Maire, J., Marchis, F., Marois, C., Millar-Blanchaer, M., Morzinski, K., Nunez, A., Oppenheimer, R., Palmer, D., Pazder, J., Perrin, M., Poyneer, L. A., Pueyo, L., Quiroz, C., Rantakyro, F., Reshetov, V., Saddlemyer, L., Sadakuni, N., Savransky, D., Serio, A., Sivaramakrishnan, A., Smith, M., Soummer, R., Thomas, S., Wallace, J. K., Wang, J., Weiss, J., Wiktorowicz, S., and Wolff, S. G., "The Gemini planet imager: first light and commissioning," in [*Adaptive Optics Systems IV*], Marchetti, E., Close, L. M., and Vran, J.-P., eds., *Society of Photo-Optical Instrumentation Engineers (SPIE) Conference Series* **9148**, 91480J (Aug. 2014).

[8] Beuzit, J.-L., Feldt, M., Dohlen, K., Mouillet, D., Puget, P., Wildi, F., Abe, L., Antichi, J., Baruffolo, A., Baudoz, P., Boccaletti, A., Carbillet, M., Charton, J., Claudi, R., Downing, M., Fabron, C., Feautrier, P., Fedrigo, E., Fusco, T., Gach, J.-L., Gratton, R., Henning, T., Hubin, N., Joos, F., Kasper, M., Langlois, M., Lenzen, R., Moutou, C., Pavlov, A., Petit, C., Pragt, J., Rabou, P., Rigal, F., Roelfsema, R., Rousset, G., Saisse, M., Schmid, H.-M., Stadler, E., Thalmann, C., Turatto, M., Udry, S., Vakili, F., and Waters, R., "SPHERE: a 'Planet Finder' instrument for the VLT," in [*Ground-based and Airborne Instrumentation for Astronomy II*], McLean, I. S. and Casali, M. M., eds., *Society of Photo-Optical Instrumentation Engineers (SPIE) Conference Series* **7014**, 701418 (July 2008).

[9] Groff, T. D., Kasdin, N. J., Limbach, M. A., Galvin, M., Carr, M. A., Knapp, G., Brandt, T., Loomis, C., Jarosik, N., Mede, K., McElwain, M. W., Leviton, D. B., Miller, K. H., Quijada, M. A., Guyon, O., Jovanovic, N., Takato, N., and Hayashi, M., "The CHARIS IFS for high contrast imaging at Subaru," in [*Techniques and Instrumentation for Detection of Exoplanets VII*], Shaklan, S., ed., *Society of Photo-Optical Instrumentation Engineers (SPIE) Conference Series* **9605**, 96051C (Sept. 2015).

[10] Skemer, A. J., Hinz, P., Montoya, M., Skrutskie, M. F., Leisenring, J., Durney, O., Woodward, C. E., Wilson, J., Nelson, M., Bailey, V., Defrere, D., and Stone, J., "First light with ALES: A 2-5 micron adaptive optics Integral Field Spectrograph for the LBT," in [*Techniques and Instrumentation for Detection of Exoplanets VII*], Shaklan, S., ed., *Society of Photo-Optical Instrumentation Engineers (SPIE) Conference Series* **9605**, 96051D (Sept. 2015).

[11] Bowler, B. P., "Imaging Extrasolar Giant Planets," **128**, 102001 (Oct. 2016).

[12] Stone, J. M., Skemer, A. J., Hinz, P. M., Bonavita, M., Kratter, K. M., Maire, A.-L., Defrere, D., Bailey, V. P., Spalding, E., Leisenring, J. M., Desidera, S., Bonnefoy, M., Biller, B., Woodward, C. E., Henning, T., Skrutskie, M. F., Eisner, J. A., Crepp, J. R., Patience, J., Weigelt, G., De Rosa, R. J., Schlieder, J., Brandner, W., Apai, D., Su, K., Ertel, S., Ward-Duong, K., Morzinski, K. M., Schertl, D., Hofmann, K.-H., Close, L. M., Brems, S. S., Fortney, J. J., Oza, A., Buenzli, E., and Bass, B., "The LEECH Exoplanet Imaging Survey: Limits on Planet Occurrence Rates under Conservative Assumptions," **156**, 286 (Dec. 2018).

[13] Chauvin, G., Vigan, A., Bonnefoy, M., Desidera, S., Bonavita, M., Mesa, D., Boccaletti, A., Buenzli, E., Carson, J., Delorme, P., Hagelberg, J., Montagnier, G., Mordasini, C., Quanz, S. P., Segransan, D., Thalmann, C., Beuzit, J. L., Biller, B., Covino, E., Feldt, M., Girard, J., Gratton, R., Henning, T., Kasper, M., Lagrange, A. M., Messina, S., Meyer, M., Mouillet, D., Moutou, C., Reggiani, M., Schlieder, J. E., and Zurlo, A., "The VLT/NaCo large program to probe the occurrence of exoplanets and brown dwarfs at wide orbits. II. Survey description, results, and performances," **573**, A127 (Jan. 2015).

[14] Galicher, R., Marois, C., Macintosh, B., Zuckerman, B., Barman, T., Konopacky, Q., Song, I., Patience, J., Lafrenière, D., Doyon, R., and Nielsen, E. L., "The International Deep Planet Survey. II. The frequency of directly imaged giant exoplanets with stellar mass," **594**, A63 (Oct. 2016).

[15] Nielsen, E. L., De Rosa, R. J., Macintosh, B., Wang, J. J., Ruffio, J.-B., Chiang, E., Marley, M. S., Saumon, D., Savransky, D., Ammons, S. M., Bailey, V. P., Barman, T., Blain, C., Bulger, J., Burrows, A., Chilcote, J., Cotten, T., Czekala, I., Doyon, R., Duchêne, G., Esposito, T. M., Fabrycky, D., Fitzgerald, M. P., Follette, K. B., Fortney, J. J., Gerard, B. L., Goodsell, S. J., Graham, J. R., Greenbaum, A. Z., Hibon, P., Hinkley, S., Hirsch, L. A., Hom, J., Hung, L.-W., Dawson, R. I., Ingraham, P., Kalas, P., Konopacky, Q., Larkin, J. E., Lee, E. J., Lin, J. W., Maire, J., Marchis, F., Marois, C., Metchev, S., Millar-Blanchaer, M. A., Morzinski, K. M., Oppenheimer, R., Palmer, D., Patience, J., Perrin, M., Poyneer, L., Pueyo, L.,

Rafikov, R. R., Rajan, A., Rameau, J., Rantakyrö, F. T., Ren, B., Schneider, A. C., Sivaramakrishnan, A., Song, I., Soummer, R., Tallis, M., Thomas, S., Ward-Duong, K., and Wolff, S., "The Gemini Planet Imager Exoplanet Survey: Giant Planet and Brown Dwarf Demographics from 10 to 100 au," **158**, 13 (July 2019).

[16] Marley, M. S., Fortney, J. J., Hubickyj, O., Bodenheimer, P., and Lissauer, J. J., "On the Luminosity of Young Jupiters," **655**, 541–549 (Jan. 2007).

[17] Burrows, A., Marley, M., Hubbard, W. B., Lunine, J. I., Guillot, T., Saumon, D., Freedman, R., Sudarsky, D., and Sharp, C., "A Nongray Theory of Extrasolar Giant Planets and Brown Dwarfs," **491**, 856–875 (Dec. 1997).

[18] Chabrier, G., "The Galactic Disk Mass Budget. I. Stellar Mass Function and Density," **554**, 1274–1281 (June 2001).

[19] Baraffe, I., Chabrier, G., Barman, T. S., Allard, F., and Hauschildt, P. H., "Evolutionary models for cool brown dwarfs and extrasolar giant planets. The case of HD 209458," **402**, 701–712 (May 2003).

[20] Berardo, D., Cumming, A., and Marleau, G.-D., "The Evolution of Gas Giant Entropy During Formation by Runaway Accretion," **834**, 149 (Jan. 2017).

[21] Wagner, K., Follete, K. B., Close, L. M., Apai, D., Gibbs, A., Keppler, M., Müller, A., Henning, T., Kasper, M., Wu, Y.-L., Long, J., Males, J., Morzinski, K., and McClure, M., "Magellan Adaptive Optics Imaging of PDS 70: Measuring the Mass Accretion Rate of a Young Giant Planet within a Gapped Disk," **863**, L8 (Aug. 2018).

[22] Haffert, S. Y., Bohn, A. J., de Boer, J., Snellen, I. A. G., Brinchmann, J., Girard, J. H., Keller, C. U., and Bacon, R., "Two accreting protoplanets around the young star PDS 70," *Nature Astronomy* **3**, 749–754 (June 2019).

[23] Eriksson, S. C., Asensio Torres, R., Janson, M., Aoyama, Y., Marleau, G.-D., Bonnefoy, M., and Petrus, S., "Strong Hα emission and signs of accretion in a circumbinary planetary mass companion from MUSE," **638**, L6 (June 2020).

[24] Hartmann, L., Herczeg, G., and Calvet, N., "Accretion onto Pre-Main-Sequence Stars," **54**, 135–180 (Sept. 2016).

[25] Manara, C. F., Frasca, A., Alcalá, J. M., Natta, A., Stelzer, B., and Testi, L., "An extensive VLT/X-shooter library of photospheric templates of pre-main sequence stars," **605**, A86 (Sept. 2017).

[26] Fung, J., Zhu, Z., and Chiang, E., "Circumplanetary Disk Dynamics in the Isothermal and Adiabatic Limits," **887**, 152 (Dec. 2019).

[27] Natta, A., Testi, L., Muzerolle, J., Randich, S., Comerón, F., and Persi, P., "Accretion in brown dwarfs: An infrared view," **424**, 603–612 (Sept. 2004).

[28] Alcalá, J. M., Natta, A., Manara, C. F., Spezzi, L., Stelzer, B., Frasca, A., Biazzo, K., Covino, E., Randich, S., Rigliaco, E., Testi, L., Comerón, F., Cupani, G., and D'Elia, V., "X-shooter spectroscopy of young stellar objects. IV. Accretion in low-mass stars and substellar objects in Lupus," **561**, A2 (Jan. 2014).

[29] Aoyama, Y., Ikoma, M., and Tanigawa, T., "Theoretical Model of Hydrogen Line Emission from Accreting Gas Giants," **866**, 84 (Oct. 2018).

[30] Aoyama, Y. and Ikoma, M., "Constraining Planetary Gas Accretion Rate from Hα Line Width and Intensity: Case of PDS 70 b and c," **885**, L29 (Nov. 2019).

[31] Aoyama, Y., Marleau, G.-D., Mordasini, C., and Ikoma, M., "Spectral appearance of the planetary-surface accretion shock: Global spectra and hydrogen-line profiles and fluxes," *arXiv e-prints* , arXiv:2011.06608 (Nov. 2020).

[32] Marleau, G. D., Aoyama, Y., Kuiper, R., Follette, K., Turner, N. J., Cugno, G., Manara, C. F., Haffert, S. Y., Kitzmann, D., Ringqvist, S. C., Wagner, K. R., van Boekel, R., Sallum, S., Janson, M., Schmidt, T. O. B., Venuti, L., Lovis, C., and Mordasini, C., "Accreting protoplanets: Spectral signatures and magnitude of gas and dust extinction at H α," **657**, A38 (Jan. 2022).

[33] Briesemeister, Z., Sallum, S., Skemer, A., Stelter, R. D., Hinz, P., and Brandt, T., "End-to-end simulation of the SCALES integral field spectrograph," in [*Ground-based and Airborne Instrumentation for Astronomy VIII*], Evans, C. J., Bryant, J. J., and Motohara, K., eds., *Society of Photo-Optical Instrumentation Engineers (SPIE) Conference Series* **11447**, 114474Z (Dec. 2020).

[34] Betti, S. K., Follette, K. B., Ward-Duong, K., Aoyama, Y., Marleau, G. D., Bary, J., Robinson, C., Janson, M., Balmer, W., Chauvin, G., and Palma-Bifani, P., "Near-infrared Accretion Signatures from the Circumbinary Planetary-mass Companion Delorme 1 (AB)b," **935**, L18 (Aug. 2022).

[35] Harries, T., "TORUS: Radiation transport and hydrodynamics code." Astrophysics Source Code Library, record ascl:1404.006 (Apr. 2014).

[36] Lord, S. D., "A new software tool for computing Earth's atmospheric transmission of near- and far-infrared radiation." NASA Technical Memorandum 103957 (Dec. 1992).

[37] Morris, B. M., Tollerud, E., Sipőcz, B., Deil, C., Douglas, S. T., Berlanga Medina, J., Vyhmeister, K., Smith, T. R., Littlefair, S., Price-Whelan, A. M., Gee, W. T., and Jeschke, E., "astroplan: An Open Source Observation Planning Package in Python," **155**, 128 (Mar. 2018).